International Journal of Science and Engineering Invention (IJSEI)
Volume 11, Issue 07, August 2025
https://doi.org/10.23958/ijsei/vol11-i07/288

Research Article

Optimizing Deloaded Solar PV Plants for Frequency Regulation: A Case Study on the IEEE 9-Bus System

Brian Wamukoya

Jomo Kenyatta University of Agriculture and Technology, Kenya.

*Corresponding Author: Brian Wamukoya; *wamukoya.brian2023@students.jkuat.ac.ke*

Received 16 June 2025; Accepted 13 July 2025; Published 05 August 2025

Abstract

The integration of solar photovoltaic power plants (SPVPPs) into power systems reduces grid inertia, challenging frequency stability during contingencies. This paper evaluates a deloaded SPVPP with fast frequency response (FFR) capability at 34% PV penetration in a modified IEEE 9-bus system. Dynamic simulations demonstrate that while a substantial 21.40% deloading level improves frequency response, the enhancements are modest - yielding just 0.42% better RoCoF (0.7824 Hz/s vs 0.7857 Hz/s) and 0.17% higher nadir (57.13 Hz vs 57.03 Hz) compared to 0% PV penetration. The optimization process achieved only a 2.18% reduction in required deloading, highlighting limited gains from reserve tuning. Economic analysis reveals a 4.85% up-regulation cost relative to generation revenue. While the proposed strategy maintains frequency within limits despite 24% inertia reduction, its marginal gains in this small test system suggest potentially greater effectiveness in larger systems where sufficient baseline inertia exists to complement the SPVPP's regulation capabilities. The study provides critical insights into the system-scale considerations for implementing SPVPP-based frequency regulation.

Keywords: ***Deloading, fast frequency response, frequency regulation, inertia, solar PV power plant***

Introduction

The rapid integration of variable renewable energy sources (VRES), particularly solar photovoltaic (PV) systems, into modern power grids has introduced new challenges in dynamically handling post-disturbance frequency stability. Unlike conventional synchronous generators (SGs), grid-connected solar PV power plants (SPVPPs) lack inherent inertia and governor response, which are critical for maintaining system frequency during power imbalances [1,2,3]. As solar penetration increases, the displacement of synchronous generation reduces system inertia, exacerbating frequency deviations during contingencies [4],[5]. Reduced system inertia increases the dynamism of the power grid, lowers its resilience, and makes it more vulnerable to significant frequency fluctuations even in response to minor disturbances [6]. Moreover, reduced inertia limits the time available to address power imbalances, emphasizing the need for rapid frequency response mechanisms in low-inertia grids to preserve frequency stability [7],[8]**.** To address the low inertia problem, deloaded operation (below MPPT) of SPVPPs with fast frequency response (FFR) capability has emerged as a promising solution to provide rapid primary frequency regulation without delay [9],[10].

Recent studies have demonstrated that deloaded SPVPPs can contribute to frequency stability by maintaining active power reserves [7],[11],[12]. However, determining the optimal deloading level remains a critical challenge, as excessive reserves undermine plant economic efficiency while insufficient reserves may fail to provide adequate frequency support, potentially compromising frequency stability [13]. Various optimization techniques, such as particle swarm optimization (PSO) and genetic algorithm (GA) have been explored to determine the trade-off between frequency response performance and operational costs [7],[11]. Despite these advancements, most studies have focused on medium- to large-scale power systems, with limited application or validation in small-scale systems. Consequently, the effectiveness of such frequency regulation strategies in smaller networks-such as microgrids or test systems like the IEEE 9-bus-remains largely unexplored and warrants further investigation.

This paper presents a comprehensive evaluation of frequency regulation using deloaded SPVPPs through dynamic simulations on a modified IEEE 9-bus test system -a small-scale network commonly used for academic and research purposes. Addressing the gap in existing literature, which predominantly focuses on medium- and large-scale systems, this study makes three key contributions: First, it demonstrates the viability of applying deloaded SPVPPs for frequency regulation in small-scale power systems by quantifying the frequency response improvements achievable under different solar penetration levels (0% and 34%). Second, it investigates the economic trade-offs of deloading by assessing up-regulation costs associated with maintaining active power reserves. Third, it explores the scalability constraints of the approach by analysing how marginal improvements in frequency response relate to increasing reserve capacity requirements.

The remainder of this paper is structured as follows: Section 2 outlines the dynamic modelling of the SPVPP and the development of a multi-objective optimization framework. Section 3 details the

simulation environment and section 4 presents the results, along with a discussion of the findings. Lastly, Section 5 provides the conclusion and suggests directions for future research

Methods

2.1 Modelling of a Deloaded SPV Power Plant

Solar photovoltaic power plants (SPVPPs) are conventionally operated in Maximum Power Point Tracking (MPPT) mode to extract maximum available power, leaving no reserve. However, recent advancements in power electronics and control have enabled SPVPPs to participate in frequency control [14]. SPVPPs can operate in a deloaded mode, where they are intentionally run below their optimal power point- P_{mpp} to create a reserve margin- $P_{deloaded}$ provided by (1). By adjusting the DC-side operating voltage to a higher value ($V_{red} = V_{mpp} + V_{deload}$) as shown in Fig. 1, the SPVPP generates reduced power- P_{red}, freeing up a reserve that can be quickly deployed to support grid frequency as FFR, mimicking SGs [15].

$$P_{deloaded} = P_{mpp} - P_{red} \quad (1)$$

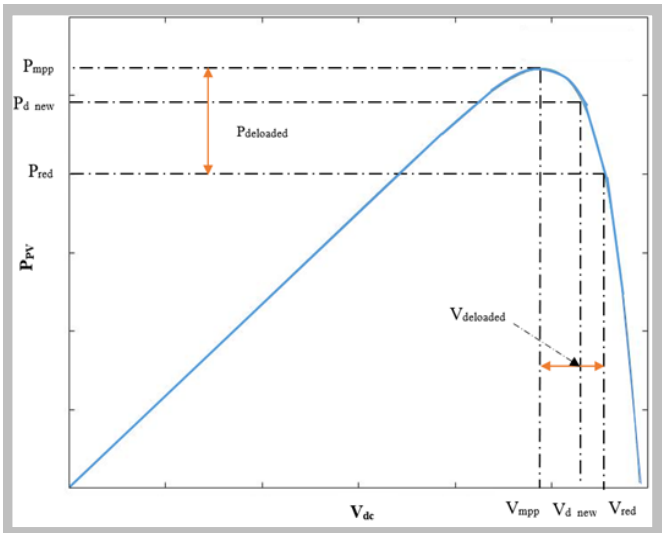

Fig. 1: Deloaded SPVPP Operation

This dynamic operation was modelled and simulated in DIgSILENT PowerFactory by implementing the active power controller shown in Fig. 2 using DSL [16]. During a contingency, the reserved power ($P_{deloaded}$) is released by adjusting the SPV array's DC voltage (V_{red}) based on frequency deviation (Δf). A control signal proportional to Δf reduces V_{red}, increasing the active power output to a new level- P_{d_new}. This active power control, implemented in DIgSILENT Simulation Language (DSL), shifts the operating voltage to a new point- V_{d_new} given by (2), enabling rapid active power support during frequency disturbances [17]. The PI controller receives the error signal and computes a control signal to adjust the converter direct axis current reference- I_{dref} which is responsible for modulating active power injection. The value of I_{dref} changes proportionally with changes in frequency.

$$V_{d\_new} = V_{red} - K_g\Delta f = V_{mpp} + V_{deload} - K_g\Delta f \quad (2)$$

Where K_g represents the proportional gain constant.

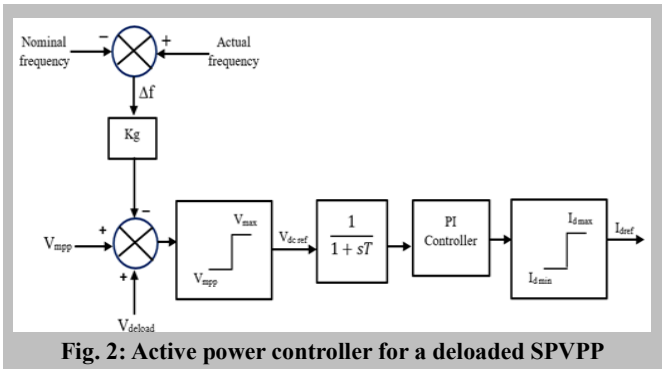

Fig. 2: Active power controller for a deloaded SPVPP

2.2 Optimization Problem Formulation

A multi-objective optimization problem was developed to simultaneously reduce total power system costs and environmental emissions in a grid with solar PV integration

Objective 1: Operation Cost minimization

The first objective function focuses on minimizing operational expenses, which include both conventional generation costs and the additional costs associated with maintaining solar PV reserves through deloading, as mathematically represented in equation (5) [11] ,

$$f = \sum_{i=1}^{ng}\left(a_i + b_iP_{gi} + c_iP_{gi}^2\right) + C_{PV} \times P_{PV} + C_{ur} \times P_{dl} \quad (5)$$

Here, a_i, b_i and c_i denote cost coefficients for the i^{th} SG while ng is the total number of generators. P_{gi} respresnts active power output of the i^{th} generator, P_{PV} is the SPV output power, C_{PV} is the unit cost of SPV generation, C_{ur} is the unit cost of upregulation and P_{dl} is the reserve capacity for deloaded SPV power plants. In this study, the SG coefficients were set as; a= 0.1 $/h, b= 0.3 $/MWh and c= 0.2 $/MW^{2}h. For SPV, C_{PV} was 61.8 $/MWh and C_{ur} was 11 $/MWh as in [12].

SPV output power, P_{PV} and deloaded margin, P_{dl} can be written as:

$$P_{PV} = P_G \times pen \times \left(1 - \frac{d}{100}\right) \quad (7)$$

$$P_{dl} = P_G \times pen \times \frac{d}{100} \quad (8)$$

Here, *pen* represents SPVPP penetration level and *d* – the deloading level given by (9) and (10) respectively [15]:

$$pen = \frac{PV\ output\ at\ MPPT}{Total\ power\ generated\ by\ the\ grid} \quad (9)$$

$$d = \frac{P_{dl}}{P_G \times pen} \times 100 = \frac{P_{dl}}{P_{PV} + P_{dl}} \times 100 \quad (10)$$

Where P_G- aggregate power produced by all committed generators.

The first objective function- F_C was formulated as in (11).

$$Minimize, F_c = \sum_{i=1}^{ng}\left(a_i + b_iP_{gi} + c_iP_{gi}^2\right) + C_{PV} \times P_G \times pen \times \left(1 - \frac{d}{100}\right) + C_{ur} \times P_G \times pen \times \frac{d}{100} \quad (11)$$

Objective 2: Ecological Emissions reduction

Amid growing climate change concerns from greenhouse gas (GHG) emissions, reducing fossil-fuelled power plant emissions has become critical. Carbon credit mechanisms now incentivize utilities to cut GHG output. Accordingly, the second objective function *Fe*- minimizing emissions costs (in $/h)-was formulated as shown in (12) [18].

$$F_e = \sum_{i=1}^{ng} \gamma_i P_{Gi}^2 + \beta_i P_{Gi} + \alpha_i + \zeta_i exp(\lambda_i P_{Gi}) \times C_{tax} \quad (12)$$

Here C_{tax} denotes the carbon tax (in \$/t). γ_i, β_i, α_i, ζ_i and λ_i represent emission coefficients for the i^{th} generator.

Aggregate Objective function

The overall objective function-F_T given in (13) was developed by merging the $1^{st}$and 2^{nd} objective functions using a weight factor (ω=0.5) to equally prioritize operational cost and emission reduction [19].

$$Minimize, F_T = \omega \times F_c + [(1-\omega) \times F_e] \quad (13)$$

Constraints

The proposed multi-objective optimization is constrained by the following system limitations:

Power balance: The total active power generated must equal the sum of total load connected and system losses as in (14).

$$\sum_{i=1}^{ng} P_{gi} + P_{PV} = P_{Load} + P_{Loss} \quad (14)$$

Deloading level (d): Defines the reserve margin for an SPVPP. While higher reserves (d) enhance flexibility, excessive deloading is economically impractical due to significant revenue losses from curtailed power. Thus, the SPV system operates within a maximum feasible deloading limit- d_{max}, as specified in (15), where d > 0 ensures active reserve availability.

$$d \leq d_{max} \leq 20\% \quad (15)$$

Power generation limits: Active and reactive power output limit of SGs and SPVPPs must be adhered to as provided in (16) & (17) respectively

$$P_{gi}^{min} \leq P_{gi} \leq P_{gi}^{max} \; for \; i = 1, 2, \ldots \ldots n \quad (16a)$$

$$Q_{gi}^{min} \leq Q_{gi} \leq Q_{gi}^{max} \; for \; i = 1, 2, \ldots \ldots n \quad (16b)$$

Where P_{gi}^{min} and P_{gi}^{max}represent least and maximum possible active power output for the i^{th} SG for n number of SGs. Q_{gi}^{min} and Q_{gi}^{max} represent least and maximum possible reactive power output for the i^{th} SG for n number of SGs.

$$P_{PVj}^{min} \leq P_{PVj} \leq P_{PVj}^{max} \; for \; j = 1, 2, \ldots \; k \quad (17a)$$

$$Q_{PVj}^{min} \leq Q_{PVj} \leq Q_{PVj}^{max} \; for \; j = 1, 2, \ldots \; k \quad (17b)$$

Where P_{PVj}^{min} and P_{PVj}^{max} represent least and maximum possible active power output for the j^{th} SPVPP for k number of SPVPPs. Q_{PVj}^{min} and Q_{PVj}^{max} represent least and maximum possible reactive power output for the j^{th} SPVPP for k number of SPVPPs.

Power system frequency stability metrics: Dynamic values of Frequency nadir-$f_{\_nadir}$ and RoCoF are constrained within prescribed limits for dynamic simulations for frequency secure operations as given in (18) and (19) respectively.

$$f\_nadir \geq f\_\min \quad (18)$$

$$RoCoF \leq RoCoF^{max} \quad (19)$$

Here $f_{\_min}$- minimum post disturbance allowable frequency, $f_{\_nadir}$ – minimum frequency reached during dynamic simulation, $RocoF^{max}$ –maximum allowable post disturbance rate of change of frequency. After a frequency event, RoCoF is approximated using (20)

$$RoCoF = \frac{df}{dt} = \frac{f_0}{2} \times \frac{\Delta P}{H_{sys}} \quad (20)$$

Where f_0- nominal frequency (in hertz), ΔP – amount of power mismatch (in p.u) and H_{sys} – system inertia constant after a disturbance (in seconds).

2.3 Implementation of PSO Algorithm to Optimize SPVPP Deloading Levels

Particle Swarm Optimization (PSO) is a metaheuristic algorithm modelled after the collective behaviour of bird flocks or fish schools, introduced by Kennedy and Eberhart. It optimizes problems by iteratively adjusting a swarm of candidate solutions (particles) within a search space. Each particle updates its velocity (v) and position (x) using (21) & (22) respectively, guided by both its personal best solution and the swarm's global best. This collaborative refinement drives the particles toward optimal solutions [20].

$$v_{i+1,p} = \omega v_{i,p} + c_1 r_1 \left(P_{best} - x_{i,p}\right) + c_2 r_2 \left(G_{best} - x_{i,p}\right) \quad (21)$$

$$x_{i+1,p} = x_{i,p} + v_{i+1,p} \quad (22)$$

where p denotes the particle index and i- iteration count. P_{best} and G_{best} correspond to the particle's personal best position and swarm's global best position, respectively. The terms r_1 and r_2 are random coefficients, while c_1 and c_2 are cognitive and social acceleration constants while w denotes inertia constant.

In this work, the deloading level -d for SPVPPs is determined according to the particle position that produces the minimum fitness function value. This function captures the lowest consolidated power generation cost, where d is a key parameter in the optimization process. The algorithm parameters were configured as in [21]: swarm size- $n_p = 10$, max iterations- $n_i = 30$ and acceleration coefficients ($c_1 = 1.2$ and $c_2 = 2.0$). Fig. 3 illustrates the step-by-step optimization process for determining the optimal d value.

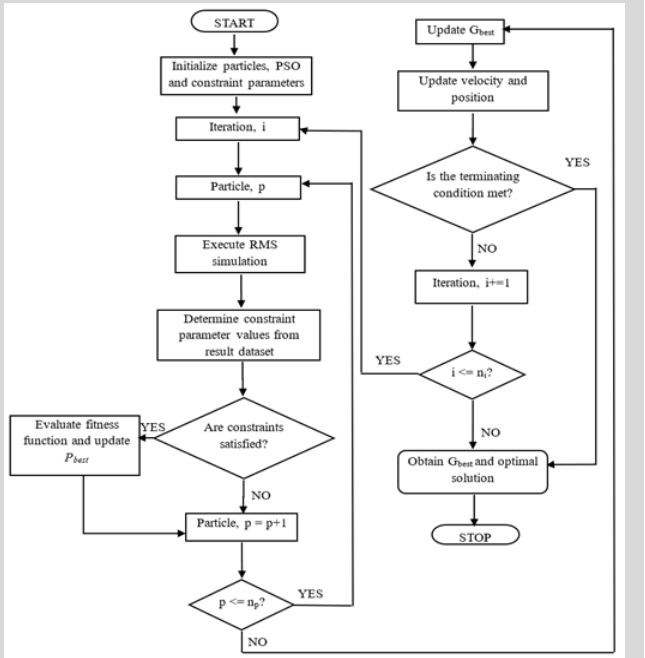

Figure 3. Flowchart for proposed optimization approach

PSO Implementation Steps

1. Initialization: PSO parameters and constraints ($f_{nadir} = 57Hz, RoCoF = 0.85Hz/s$) were defined. Particle random positions (representing deloading levels) and velocities were also initialized.
2. Simulation phase: For each particle at every iteration:
   - Time domain simulations were conducted for different penetration levels
   - SG outage was selected as a severe disturbance
   - RoCoF was calculated using (20) and f_{nadir} determined
3. Constraint validation: Compliance was verified using (14) - (19) constraints. If met, the objective function in (13) is evaluated and P_{best} is updated; otherwise, the current value is maintained.
4. Swarm update: G_{best} is selected as the optimal P_{best} i.e the one with the lowest value. Particle velocities and positions are updated using (21) & (22).
5. Termination criteria: The algorithm stops if G_{best} converges (successive differences<0.001) or max iterations – (30) is reached. Otherwise steps 2- 4 are repeated.

Case Study

3.1 Simulation Setup for IEEE 9 Bus Test System

The study used the standard IEEE 9-bus (P.M. Anderson) system to test the frequency regulation strategy. This compact test case provides an ideal platform for analysing how solar PV integration affects grid stability [22]. The system's simplicity enables clear evaluation of deloaded solar plants' ability to maintain frequency stability through FFR [23],[24].

The IEEE 9-bus test system comprises three generating units, three load centres, nine busbars, and six transmission links. The configuration features a balanced generation-load distribution, with power plants located at buses 1 through 3 and consumer loads connected to buses 5, 6, and 8, as illustrated in Fig. 4.

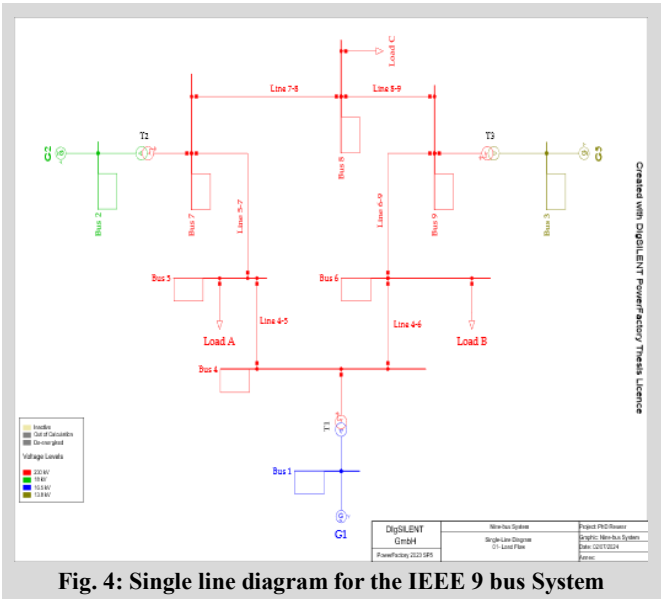

Fig. 4: Single line diagram for the IEEE 9 bus System

The generator specifications are provided in *Table 1* with supplementary system parameters including GHG emission coefficients provided in [25]. The network operates at 60 Hz with *Table 1* presenting inertia constants- *H* normalized to a100MVA base. Generator loading percentages are calculated based on individual generator rating.

Table 1. IEEE 9 Bus Generator Data

Gen	Type	Pmin -MW	Pmax - MW	Qmin- MVar	Qmax- MVar	MVA Rating	H (s)	Loading (%)
G1	Gas	60	247.5	-198	198	247.5	9.55	28.92
G2	Coal	40	163.2	-76.8	115.2	192	3.92	99.88
G3→PV	Coal	25	108.8	-51.2	76.8	128	2.77	78.34
	Total						16.2	

3.2 Simulation Procedure

Dynamic simulations were performed to assess a frequency regulation strategy using the IEEE 9-bus system in PowerFactory. The model included generator controllers (governors and AVRs) and static loads, excluding voltage and frequency dependencies. After validating the system via load flow analysis, the worst-case disturbance-generator G02 tripping at 10 seconds-was simulated for 100 seconds to obtain baseline frequency response data (0% solar PV penetration).

The model was then reset, and the SG at Bus 3 (G03) was replaced with a solar PV plant (SPVPP) of equal capacity, simulating 34% PV penetration. A Python-based PSO algorithm determined the optimal deloading level for the SPVPP to enhance frequency control during G02's outage. Key metrics evaluated included RoCoF, frequency nadir, and operational costs (generation, emissions, and up-regulation).

The optimally deloaded SPVPP's frequency response was compared to the baseline case to evaluate the strategy's effectiveness.

Results and Discussion

The frequency regulation strategy was tested on an adapted IEEE 9-bus system to evaluate its effectiveness on a small-scale power grid. The outage of generator G2-the second-largest unit (192 MVA) after the reference generator G1 (247.5 MVA)-was selected as the worst-case disturbance due to its near-maximum loading (99.9%).

4.1 Frequency Response for Static SPV

The frequency response dynamics with 34% penetration of SPV is shown in Fig. 5.

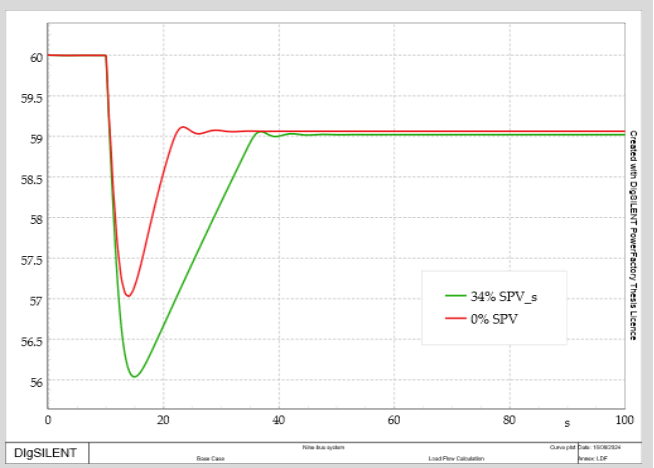

Fig. 5: Frequency response with increased penetration of SPV

Under 0% SPV penetration, the system frequency drops to 57.03 Hz with a RoCoF of 0.7857 Hz/s following the outage of generator G2. However, when generator G3 is replaced by a SPVPP of equivalent capacity-simulating 34% SPV penetration but without fast frequency response (FFR) capability-the frequency response worsens significantly. The nadir plunges to 56.04 Hz (a 1.74%

decline), while the RoCoF rises to 0.9037 Hz/s (a 15.02% increase) for the same disturbance. This degradation occurs because the SPVPP lacks the inherent inertia of the displaced synchronous generator (G3), which is crucial for stabilizing frequency during sudden generation losses.

The integration of the static SPVPP caused breaches in the frequency stability criteria outlined in Section 2.3, leading to under-frequency generator tripping and complete system failure. To analyze the system's behavior more closely, the frequency stability thresholds were temporarily relaxed, enabling the simulation to continue and assess the severity of frequency deviations when static SPVPPs were incorporated. These results highlight the destabilizing impact of deploying SPVPPs lacking FFR in low-inertia power networks, reinforcing the necessity for advanced grid-support features in renewable energy integration. Fig. 6 illustrates the system's active power response to the G2 outage, highlighting these dynamics.

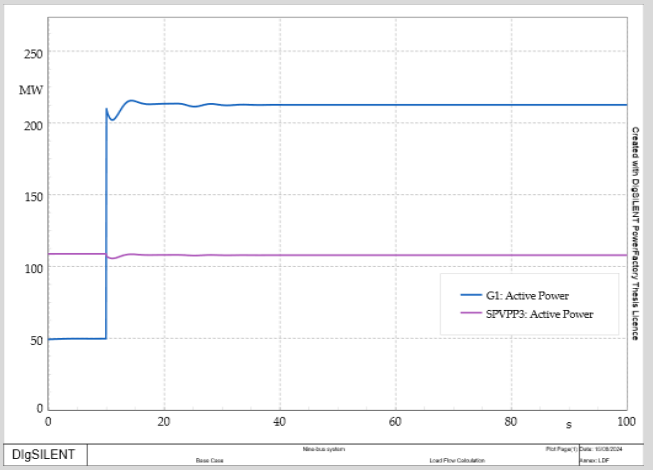

Fig. 6: Active power response with generator G2 outage

As shown in Fig. 6, the SPVPP cannot respond to the power imbalance since it lacks FFR capability. Instead, synchronous generator G1 increases its active power output to compensate for the power deficit.

4.2 Frequency Response for SPV with FFR capability

Fig. 7 illustrates the system's frequency response when generator G2 fails, now incorporating a deloaded SPVPP capable of dynamic response to power imbalances. The SPVPP's operating point matched that of the original SG (G3) it replaced, establishing the deloading level prior to optimization that is like the reserve capacity of the replaced SG (G3).

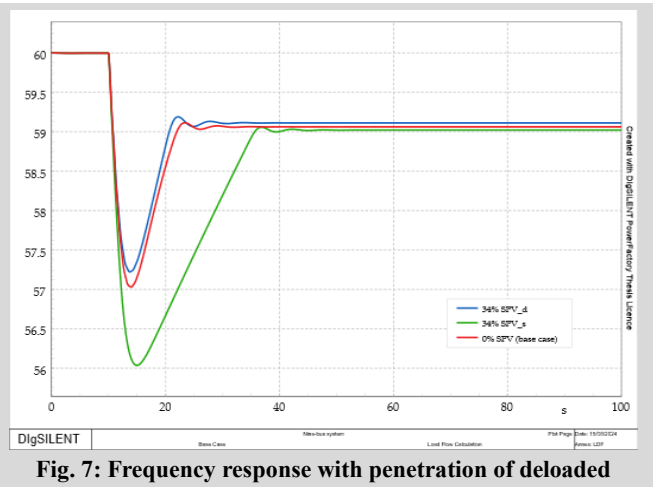

Fig. 7: Frequency response with penetration of deloaded SPVPP

The deloaded SPVPP (SPV_d) demonstrates superior frequency regulation compared to SPV penetration without FFR capability (SPV_s), evidenced by an enhanced frequency nadir of 57.22 Hz and improved RoCoF of 0.7814 Hz/s, as detailed in *Table 2.*

Table 2. Frequency stability metrics with SPVPP penetration

SPV penetration level	System Inertia Constant- H (s)	Frequency nadir (Hz)	RoCoF (Hz/s)	Deloading level (%)	Deloading capacity (MW)
0%	16.240	57.03	0.7857	-	-
34% static	12.318	56.04	0.9037	-	-
34% Deloaded	12.318	57.22	0.7814	21.88	23.8

Compared to static SPV, these results show a 2.11% higher frequency nadir and a 13.53% faster RoCoF recovery. This enhancement stems from the deloaded SPVPP's FFR capability, which enables rapid active power injection to stabilize the grid during imbalances, as demonstrated in Fig. 8.

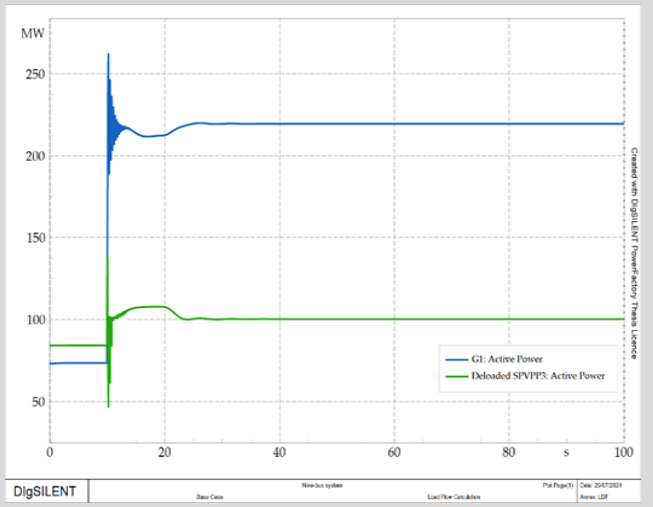

Fig. 8: Active power response of a deloaded SPVPP with generator outage

The SPVPP has a very high deloading level of 21.88% representing a capacity of 23.8 MW, proving essential for frequency stability by compensating for a 24% system inertia reduction while maintaining grid frequency within operational limits.

4.3 Optimally Deloaded SPV Penetration

Fig. 9 illustrates the PSO convergence plot. This study adopted best-per-iteration convergence plot to analyse the PSO algorithm's optimization process. Unlike global best tracking, this plot reveals search dynamics and solution diversity per iteration-crucial given the computationally intensive time-domain simulations. The nonlinear, dynamic nature of the problem caused local fitness fluctuations, making best-per-iteration insights vital for understanding how PSO navigates the constrained solution space. This granular perspective complements broader convergence trends from global best tracking.

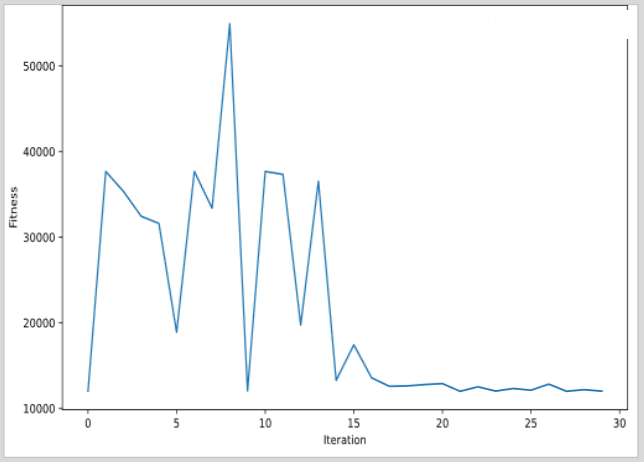

Fig. 9: PSO Convergence with 34% SPV penetration

The algorithm begins with broad exploration, causing fitness values to spike sharply as particles identify potential solution areas. Early iterations then show rapid fitness improvement before the rate of decrease gradually slows, marking the shift from exploration to exploitation. As particles converge toward optimal solutions, the fitness curve stabilizes, reaching a plateau that signals approach to near-optimal conditions. Beyond this point, further iterations yield diminishing returns in fitness improvement.

Using the PSO algorithm, at 34% SPV penetration, the optimal SPVPP deloading level was determined to be 21.40% (23.28 MW).

Fig. 10 depicts the frequency response at 21.40% deloading level. The results are compared with the response at 0% SPV.

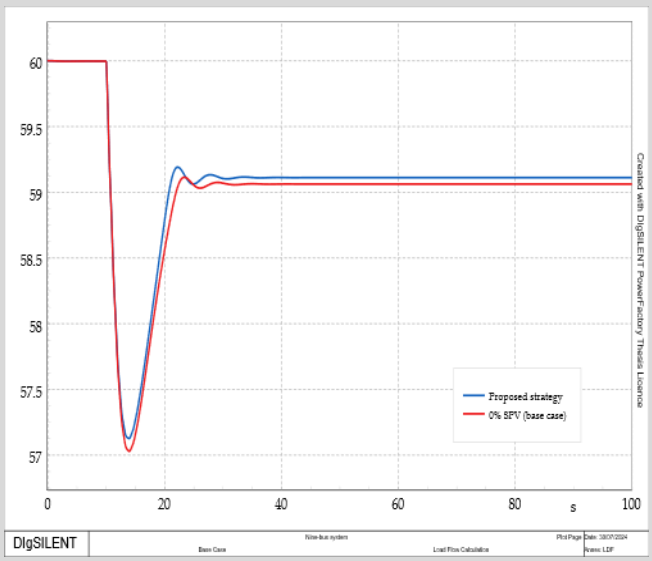

Fig. 10: Frequency response of an optimally deloaded SPVPP at 34% SPV penetration

Fig. 10 demonstrates that the optimal SPVPP deloading level of 21.40% yields slightly superior frequency response compared to 0% SPV penetration. The optimized configuration achieved RoCoF (0.7824 Hz/s) and frequency nadir (57.13 Hz) values that marginally outperformed the baseline case (0.7857 Hz/s and 57.03 Hz) while remaining within operational limits. As *Table 3* indicates, this represents modest improvements of 0.42% in RoCoF and 0.17% in frequency nadir. Notably, while the 21.40% deloading level is relatively high, it provides only slight frequency response enhancements. Furthermore, the optimization process reduced the required deloading level by just 2.18% compared to the unoptimized case.

Table 3: Optimal deloading level and capacity with SPV penetration

Variable	Value
SPV Penetration level	34%
Optimal deloading level (%)	21.40
Deloaded capacity (MW)	23.28
Deloaded SPV Generation (MW)	85.51
SG Generation (MW)	234.73
Deloaded SPV RoCoF (Hz/s)	0.7824
Deloaded SPV F_{nadir} (Hz)	57.13
RoCoF %age change	0.42
F_{nadir} %age change	0.17

The optimal aggregated operating cost was $12,018.15 per hour. *Table 4* provides the other cost categories that contribute to the aggregated operating cost.

Table 4: Summary of costs associated with optimally deloaded SPVPP

SPV Penetration level	Aggregated Operating cost ($/h)	Generation cost of SG ($/h)	Generation cost of SPV ($/h)	Ecological emission cost ($/h)	Up-regulation cost ($/h)
34%	12,018.15	6,416.81	5,284.79	60.41	256.14

In this case, the up-regulation cost (representing lost solar generation revenue) amounts to 4.85% of the SPV's total generation cost. While no universal standards exist, industry research and practical experience suggest this cost ratio must remain economically competitive with alternative frequency regulation sources. Maintaining cost-effectiveness enables solar plants to deliver affordable grid stability services while ensuring financial viability. Excessive up-regulation costs would disproportionately increase overall system operating expenses, making the solution less attractive.

The proposed approach, while applicable to smaller systems like the modified IEEE 9-bus network, shows limited performance gains through SPVPP deloading optimization. This suggests the need for validation on larger-scale power systems to properly assess its effectiveness.

Conclusion

This study demonstrates that while a deloaded SPVPP with FFR capability can improve grid stability in a modified IEEE 9-bus system, its impact remains marginal-yielding only a 0.42% improvement in RoCoF and 0.17% in frequency nadir despite a high 21.40% deloading level. The economic viability of this approach is constrained by up-regulation costs (4.85% of generation revenue), which must remain competitive with alternative frequency regulation resources. Although the proposed strategy effectively maintains frequency within permissible limits and partially compensates for lost inertia (24% reduction), the modest performance gains suggest the need for further validation on larger, more complex power systems to assess scalability. Future work could explore the design and structure of the FFR ancillary market with appropriate incentives that can stimulate generating companies to provide FRR as a critical grid resource for frequency regulations with increased penetration of SPVPPs.

References

[1] Karimi et al., "Inertia Response Improvement in AC Microgrids: A Fuzzy-Based Virtual Synchronous Generator Control," IEEE Trans Power Electron, vol. 35, no. 4, pp. 4321–4331, Apr. 2020, doi: 10.1109/TPEL.2019.2937397.

[2] A. Bonfiglio, M. Invernizzi, A. Labella, and R. Procopio, "Design and Implementation of a Variable Synthetic Inertia Controller for Wind Turbine Generators," IEEE Transactions on Power Systems, vol. 34, no. 1, pp. 754–764, Jan. 2019, doi: 10.1109/TPWRS.2018.2865958.

[3] P. Vorobev, D. M. Greenwood, J. H. Bell, J. W. Bialek, P. C. Taylor, and K. Turitsyn, "Deadbands, Droop, and Inertia Impact on Power System Frequency Distribution," IEEE Transactions on Power Systems, vol. 34, no. 4, pp. 3098–3108, Jul. 2019, doi: 10.1109/TPWRS.2019.2895547.

[4] P. Denholm, T. Mai, R. W. Kenyon, B. Kroposki, and M. O. Malley, "Inertia and the Power Grid : A Guide Without the Spin," no. May, 2020, [Online]. Available: https://www.nrel.gov/docs/fy20osti/73856.pdf

[5] N. Nguyen, D. Pandit, R. Quigley, and J. Mitra, "Frequency Response in the Presence of Renewable Generation: Challenges and Opportunities," IEEE Open Access Journal of Power and Energy, vol. 8, pp. 543–556, 2021, doi: 10.1109/OAJPE.2021.3118393.

[6] D.; Pombo, D. A.; Sørensen, and J. Martinez-Rico, "Is Real Inertia Always Better? Synchronous Condensers, Fast Frequency Response, and Virtual Inertia in Isolated Hybrid Power Systems," Madeira: Proceedings of 6th Hybrid Power Systems Workshop, Apr. 2022. Accessed: Jun. 05, 2024. [Online]. Available: https://backend.orbit.dtu.dk/ws/portalfiles/portal/275009622/3A_2_HYB22_018_paper_Pombo_Daniel.pdf

[7] B. K. Wamukoya, K. K. Kaberere, C. M. Muriithi, and K. Murang'a, "Optimal deployment of solar PV power plants as fast frequency response source for a frequency secure low inertia power grid," Bulletin of Electrical Engineering and Informatics, vol. 14, no. 1, pp. 83–95, 2025, doi: 10.11591/eei.v14i1.8548.

[8] L. Meng et al., "Fast Frequency Response from Energy Storage Systems - A Review of Grid Standards, Projects and Technical Issues," IEEE Trans Smart Grid, vol. 11, no. 2, pp. 1566–1581, Mar. 2020, doi: 10.1109/TSG.2019.2940173.

[9] B. K. Wamukoya, C. M. Muriithi, and K. K. Kaberere, "Improving frequency regulation for future low inertia power grids: a review," Bulletin of Electrical Engineering and Informatics, vol. 13, no. 1, pp. 76–87, Feb. 2024, doi: 10.11591/eei.v13i1.5873.

[10] S. Lining, Q. Xiaohui, Z. Shang, Z. Yantao, J. Yilang, and H. Yi, "Fast frequency response of inverter-based resources and its impact on system frequency characteristics," Global Energy Interconnection, pp. 475–485, 2020, doi: 10.1016/j.gloei.2020.11.007.

[11] I. Mahmud, N. Al Masood, and A. Jawad, "Optimal deloading of PV power plants for frequency control: A techno-economic assessment," Electric Power Systems Research, vol. 221, no. January, p. 109457, 2023, doi: 10.1016/j.epsr.2023.109457.

[12] A. Jawad and N. Al Masood, "A systematic approach to estimate the frequency support from large-scale PV plants in a renewable integrated grid," Energy Reports, vol. 8, pp. 940–954, 2022, doi: 10.1016/j.egyr.2021.12.017.

[13] A. Fernández-Guillamón, E. Gómez-Lázaro, E. Muljadi, and Á. Molina-García, "Power systems with high renewable energy sources: A review of inertia and frequency control strategies over time," Renewable and Sustainable Energy Reviews, vol. 115, p. 109369, Nov. 2019, doi: 10.1016/j.rser.2019.109369.

[14] R. Rajan, F. M. Fernandez, and Y. Yang, "Primary frequency control techniques for large-scale PV-integrated power systems: A review," Jul. 01, 2021, Elsevier Ltd. doi: 10.1016/j.rser.2021.110998.

[15] C. Rahmann and A. Castillo, "Fast frequency response capability of photovoltaic power plants: The necessity of new grid requirements and definitions," Energies (Basel), vol. 7, no. 10, pp. 6306–6322, 2014, doi: 10.3390/en7106306.

[16] P. Pachanapan, "Dynamic Modelling and Simulation of Power Electronic Converter in DIgSILENT Simulation Language (DSL): Islanding Operation of Microgrid System with Multi-energy Sources," 2021, pp. 67–93. doi: 10.1007/978-3-030-54124-8_3.

[17] P. P. Zarina, S. Mishra, and P. C. Sekhar, "Exploring frequency control capability of a PV system in a hybrid PV-rotating machine-without storage system," International Journal of Electrical Power and Energy Systems, vol. 60, pp. 258–267, 2014, doi: 10.1016/j.ijepes.2014.02.033.

[18] S. Albatran, S. Harasis, M. Ialomoush, Y. Alsmadi, and M. Awawdeh, "Realistic Optimal Power Flow of a Wind-Connected Power System With Enhanced Wind Speed Model," IEEE Access, vol. 8, pp. 176973–176985, 2020, doi: 10.1109/ACCESS.2020.3027065.

[19] Y. Cui, Z. Geng, Q. Zhu, and Y. Han, "Review: Multi-objective optimization methods and application in energy saving," Energy, vol. 125, pp. 681–704, Apr. 2017, doi: 10.1016/J.ENERGY.2017.02.174.

[20] A. G. Gad, "Particle Swarm Optimization Algorithm and Its Applications: A Systematic Review," Archives of Computational Methods in Engineering, vol. 29, no. 5, pp. 2531–2561, Aug. 2022, doi: 10.1007/s11831-021-09694-4.

[21] A. P. Piotrowski, J. J. Napiorkowski, and A. E. Piotrowska, "Population size in Particle Swarm Optimization," Swarm Evol Comput, vol. 58, Nov. 2020, doi: 10.1016/j.swevo.2020.100718.

[22] S. Peyghami, P. Davari, M. Fotuhi-Firuzabad, and F. Blaabjerg, "Standard Test Systems for Modern Power System Analysis: An Overview," IEEE Industrial Electronics Magazine, vol. 13, no. 4, pp. 86–105, Dec. 2019, doi: 10.1109/MIE.2019.2942376.

[23] N. U. Putri, F. Rossi, A. Jayadi, J. P. Sembiring, and H. Maulana, "Analysis of Frequency Stability with SCES's type of Virtual Inertia Control for The IEEE 9 Bus System," in 2021 International Conference on Computer Science, Information Technology, and Electrical Engineering (ICOMITEE), Banyuwangi, Indonesia: IEEE, Oct. 2021, pp. 191–196. doi: 10.1109/ICOMITEE53461.2021.9650178.

[24] K. Loji, N. Loji, and M. Kabeya, "Flexibility Assessment of a Solar PV Penetrated IEEE 9-Bus System Using Dynamic Transient Stability Evaluation," in 2022 IEEE

PES/IAS PowerAfrica, Kigali, Rwanda: IEEE, Aug. 2022, pp. 1–5. doi: 10.1109/PowerAfrica53997.2022.9905395.

[25] K. Abaci and V. Yamacli, "Differential search algorithm for solving multi-objective optimal power flow problem," International Journal of Electrical Power and Energy Systems, vol. 79, pp. 1–10, Jul. 2016, doi: 10.1016/j.ijepes.2015.12.021.